Performance and Equivalent Loads of Wind Turbines in Large Wind Farms

Andersen, Søren Juhl; Sørensen, Jens Nørkær; Mikkelsen, Robert Flemming

Published in:
Wake Conference 2017

Link to article, DOI:
10.1088/1742-6596/854/1/012001

Publication date:
2017

Document Version
Publisher's PDF, also known as Version of record

Performance and Equivalent Loads of Wind Turbines in Large Wind Farms

2017 J. Phys.: Conf. Ser. 854 012001

(http://iopscience.iop.org/1742-6596/854/1/012001)

IOP Conf. Series: Journal of Physics: Conf. Series **854** (2017) 012001 doi:10.1088/1742-6596/854/1/012001

Performance and Equivalent Loads of Wind Turbines in Large Wind Farms

Søren J. Andersen, Jens N. Sørensen, Robert F. Mikkelsen
DTU Wind Energy, Technical University of Denmark, 2800 Lyngby, Denmark
E-mail: sjan@dtu.dk

Abstract.
Ten simulations of large wind farms have been performed using a fully coupled LES and aero-elastic framework to form a database of full turbine operational conditions in terms of both production and loads. The performance is examined in terms of averaged power production and thrust, as well as 10min equivalent flapwise bending, yaw, and tilt moment loads. Certain scenarios operating below rated wind speed shows unexpected peaks in the loads. The influence on the operating conditions are examined for various parameters and compared relative to an effective power production per area.

1. Introduction

State-of-the-art in numerical simulations of wind farms is based on a combination of Large Eddy Simulations (LES) for solving the flow and the actuator line method by Sørensen and Shen [1] to model the turbines. LES have proven capable of providing detailed flow results and analysis of large wind farms, *e.g.* Calaf et al. [2], Meyers and Meneveau [3]-[4], Porté-Agel et al. [5], and Nilsson et al. [6]. Similarly, the actuator line method has proven good for modelling the turbine(s), *e.g.* Troldborg [7] and Jha et al. [8]. However, work including full coupling of the flow modelling and aero-elastic modelling for large wind farms is still scarce, but see Sørensen et al. [9], Andersen [10], Storey et al. [11], Lee et al. [12] as well as Vitsas and Meyers [10], who used a multibody approach rather than actuator lines.

However, such state-of-the-art simulations are still very computational expensive, but could potentially provide calibration data and insight into lower fidelity models, for instance the Dynamic Wake Meandering model by Larsen et al. [13]-[14].

Here, a collection of large wind farms simulations is examined in terms of both power production and aero-elastic load estimations to elucidate on the operating conditions of wind turbines deep inside large wind farms and how these conditions relate to various parameters, such as atmospheric turbulence, freestream velocity, and turbine spacing.

2. Methodology

2.1. Numerical Implementation

The simulations are performed using EllipSys3D, which solves the discretized incompressible Navier-Stokes equations with a finite volume approach in general curvilinear coordinates. EllipSys3D is formulated in pressure-velocity variables, and the pressure correction is solved through the PISO algorithm. Rhie-Chow interpolation technique is employed to avoid pressure

decoupling. The convective terms are discretized in a combination of the third order QUICK scheme and the fourth order CDS scheme in order to prevent numerical wiggles. EllipSys3D is developed at DTU, see Michelsen [15]) and Risø (Sørensen[16]).

The wind turbines are modelled by the actuator line (AL) method, see Sørensen and Shen [1]. AL applies body forces ($\boldsymbol{f}_{WT}$) along rotating lines representing the turbine blades. The imposed body forces are calculated by the aero-elastic tool, Flex5, see e.g. Øye [17].

The actuator lines are fully coupled to Flex5, hence the turbines respond directly to the turbulent inflow, see Sørensen et al. [9] for details.

The atmospheric boundary layer (ABL) is prescribed explicitly by imposing additional body forces ($\boldsymbol{f}_{pbl}$) in the flow as described by Troldborg et al. [18]. The prescribed boundary layers are here taken as a combination of a parabolic and a power law profile described by:

$$U_{pbl}(z) = \begin{cases} U_0 \cdot (c_2 z^2 + c_1 z) & z \leq \Delta_{PBL} \\ U_0 \cdot \left(\frac{z}{H_{hub}}\right)^{\alpha_{PBL}} & z > \Delta_{PBL} \end{cases} \tag{1}$$

where Δ_{PBL} determines the height, where the velocity profile changes from parabolic to power law. H_{hub} is the hub height, c_1, c_2, and α_{PBL} are shape parameters. c_1 and c_2 are calculated to ensure a smooth transition between the parabolic and the power law expression.

Atmospheric turbulence is also added through body forces ($\boldsymbol{f}_{turb}$) in a Simulations O, B, C, F, and I. The forces are added in a plane $4R$ upstream the turbine. The body forces are derived based on stochastically generated turbulence using the Mann model, see Mann [19]-[20]. The advantage of the Mann model is that second-order statistics (variance, cross-spectra, etc.) are matched to those occurring in a neutral atmosphere. The turbulence box has an extent of $179,000\text{m}\times6400\text{m}\times6400\text{m}$, which is larger than a standard Mann box in order to include very long length scales. The advantage of using body forces is that no precursor simulation is needed and it is possible to apply different turbulence intensities for the same shear.

Hence, the filtered flow field is found by solving the 3D incompressible Navier-Stokes equations with added body forces:

$$\frac{\partial \overline{\boldsymbol{V}}}{\partial t} + \overline{\boldsymbol{V}} \cdot \nabla \overline{\boldsymbol{V}} = -\frac{1}{\rho}\nabla \overline{p} + \nabla[(\nu + \nu_{SGS})\nabla \overline{\boldsymbol{V}}] + \frac{1}{\rho}\boldsymbol{f}_{WT} + \frac{1}{\rho}\boldsymbol{f}_{pbl} + \frac{1}{\rho}\boldsymbol{f}_{turb}. \tag{2}$$

The sub-grid scale (SGS) viscosity (ν_{SGS}) used in the LES is modeled using the vorticity based mixing scale by Ta Phuoc et al. [21].

2.2. Turbine

The modeled turbine is the NM80 turbine, see Madsen et al. [22]. NM80 has a radius $R = 40m$ and is rated to $2.75MW$ for $U_{hub} = 14\text{m/s}$.

The turbine includes an active controller consisting of a variable speed P-controller for small wind speeds ($U_{hub} < 14m/s$) and a PI-pitch angle controller for higher wind speeds. The controller responds continuously to the dynamic inflow as it would for a real turbine, which means that the modelled rotors are not constantly loaded and the blades pitch when the velocity is above rated.

2.3. Simulations Overview

A total of ten large wind farms have been modeled and summarized in Table 1. Each wind farm includes 16 turbines in the streamwise direction with hub height of $Z_{hub} = 2R$. Simulation O is a reference case, and identical to Simulation C except the turbines do not exert any forces on the flow, *i.e.* the turbines do not influence the flow, but statistics are extracted at the same locations for direct comparison. Cyclic boundary conditions are imposed in the lateral direction

to mimic infinitely wide farms. The main parameters are streamwise and lateral spacings (S_X, S_Y), atmospheric turbulence intensity (TI) and freestream velocity at hub height (U_0), whereas shear is kept constant in the present work. Furthermore, the blade resolution and the number of cells in the computational domain are provided. The used grids have very comparable resolution, and no stretching is applied to prevent smearing of the wakes. Five of the ten simulations have been run with an atmospheric turbulence intensity of 0%, which is an idealized situation, but enables the study of the self-generated turbulence stemming only from the turbines themselves. The simulations have been run for at least two flow throughs to flush the domain of any transients and statistics are based on $60mins$, except Simulation H, which is based on $30min$ statistics. Simulations A-C, F, and H-I constitute the same wind farm under different inflow conditions. Several of the simulations have previously been reported in Andersen et al. [23], which showed that higher order flow statistics are comparable when scaled by a representative velocity, which can be assessed directly from the power curve, both instanteneously and averaged. Simulations O, A, B, and C have previously been investigated in detail in Andersen et al. [24], who concluded that the dominant length scales responsible for the energy entrainment in large wind farms is limited by the turbine spacing.

Table 1. Overview of simulations. *No forces are applied from the turbines to the flow, but aero-elastic results are extracted similar to simulation C.

Name	U_0	TI	Shear	Spacing ($S_X \times S_Y$)	Time step	Blade resolution	Cells in grid
O	$8m/s$	15%	0.14	$12R \times 20R^*$	$0.025s$	17	$327 \cdot 10^6$
A	$8m/s$	0%	0.14	$12R \times 20R$	$0.025s$	17	$327 \cdot 10^6$
B	$8m/s$	3%	0.14	$12R \times 20R$	$0.025s$	17	$327 \cdot 10^6$
C	$8m/s$	15%	0.14	$12R \times 20R$	$0.025s$	17	$327 \cdot 10^6$
D	$8m/s$	0%	0.14	$12R \times 12R$	$0.025s$	17	$120 \cdot 10^6$
E	$15m/s$	0%	0.14	$12R \times 12R$	$0.013s$	17	$120 \cdot 10^6$
F	$15m/s$	15%	0.14	$12R \times 20R$	$0.013s$	18	$235 \cdot 10^6$
G	$8m/s$	0%	0.14	$20R \times 20R$	$0.025s$	17	$524 \cdot 10^6$
H	$20m/s$	0%	0.14	$12R \times 20R$	$0.010s$	17	$327 \cdot 10^6$
I	$20m/s$	15%	0.14	$12R \times 20R$	$0.010s$	17	$327 \cdot 10^6$

3. Results

3.1. Statistical treatment

The present analyses focus on the following quantities:

- Velocity extracted $1R$ upstream at hub height, V_{hub}
- Power production, P
- Flapwise bending moment, M_F
- Yaw moment, M_Y
- Tilt moment, M_T
- Thrust force, T

where the statistics are calculated for different 10min periods shifted by 1min within the total simulation time, *i.e.* a total of 51 periods within 60min. The equivalent loads are computed using rainflow counting with Wöhler exponents of $m = 10$ for flap and $m = 6$ for yaw and tilt.

The data have been scaled by the following quantities for all the simulations to enable a direct comparison of the relative change. Hence, all quantities are denoted by a supercript * to indicate the scaling. Table 2 contain the scalings parameters.

Table 2. Overview of scaling parameters.

Quantity	Scaling parameter
V^*_{hub}	Maximum mean velocity of all simulations.
P^*	Rated power
M^*_F	Maximum of the mean equivalent flapwise bending moment of all simulations
M^*_Y	Maximum of the mean equivalent yaw moment of all simulations
M^*_T	Maximum of the mean equivalent tilt moment of all simulations
T^*	Maximum mean thrust force of all simulations

3.2. Spatial Variability

As previously shown by Andersen et al. [25] and Andersen et al. [23] the flow statitics have generally converged after the $4th$ or $5th$ turbine, although there can be large temporal varibility. Certain simulations also yield significant spatial variability, albeit not continuously increasing or decreasing through the farm, but rather alternating around the converged level. Figure 1 shows boxplot distributions for each of the 16 turbines in Simulations *A*-*C*. The lines connect the median of the distributions to make the trend even clearer. The velocity distributions are generally converged with only minor deviations in terms of medians and spread of the distributions. The standard deviation of V_{hub} shows a larger variation with distinct peaks, *e.g.* around the $9th$ turbine. Whether the standard deviation of the velocity at a single point is representative is questionable, but it shows how numerical power estimates should include the fluctuating part, *i.e.* $P \propto (\overline{U} + u')^3$, as the turbine is capable of extracting some of the larger turbulent scales. Peaks are even more pronounced in power, flapwise bending, yaw, tilt(not shown) moments, and thrust, and they are consistently located at the $5th$, $7th$, $10th$, $12th$, and $15th$ turbine across all three simulations. In addition to the consistent location, it does not stem from the imposed atmospheric turbulence as it also occurs for Simulation *A* and the peaks are not consistent in the standard deviation of the hub height velocity.

Figure 2 shows contour of the mean streamwise velocity and inplane streamlines for simulation *A*. The particular turbines show a significant smaller wake and higher velocity in a thin, horizontal band at hub height, but there appears to be no increased lateral movement. The repeating pattern could resemble a large scale harmonic effect, and it has recently been shown by Newman et al. [26] and Andersen et al. [24] that the largest turbulent structures are limited by the turbine spacing, yet grow further into the farms.

Boxplots of power, yaw, and thrust for the remaining simulations are shown in Figure 3. Here, the effect is less pronounced, although it occurs in the yaw (and tilt) moments for a number of the simulations, *e.g.* for turbines 8, 10, and 13 in simulation *D*. However, it is hardly seen in power and thrust. This "anomaly" requires additional investigation to determine if it is a physical or numerical artifact.

3.3. Aggregated Statistics

The data is aggregated for the $7th - 16th$ turbines to yield statistics of turbines operating deep inside large wind farms, and not only statistics of the $8th$ or $11th$ turbine. Hence, a total of 510

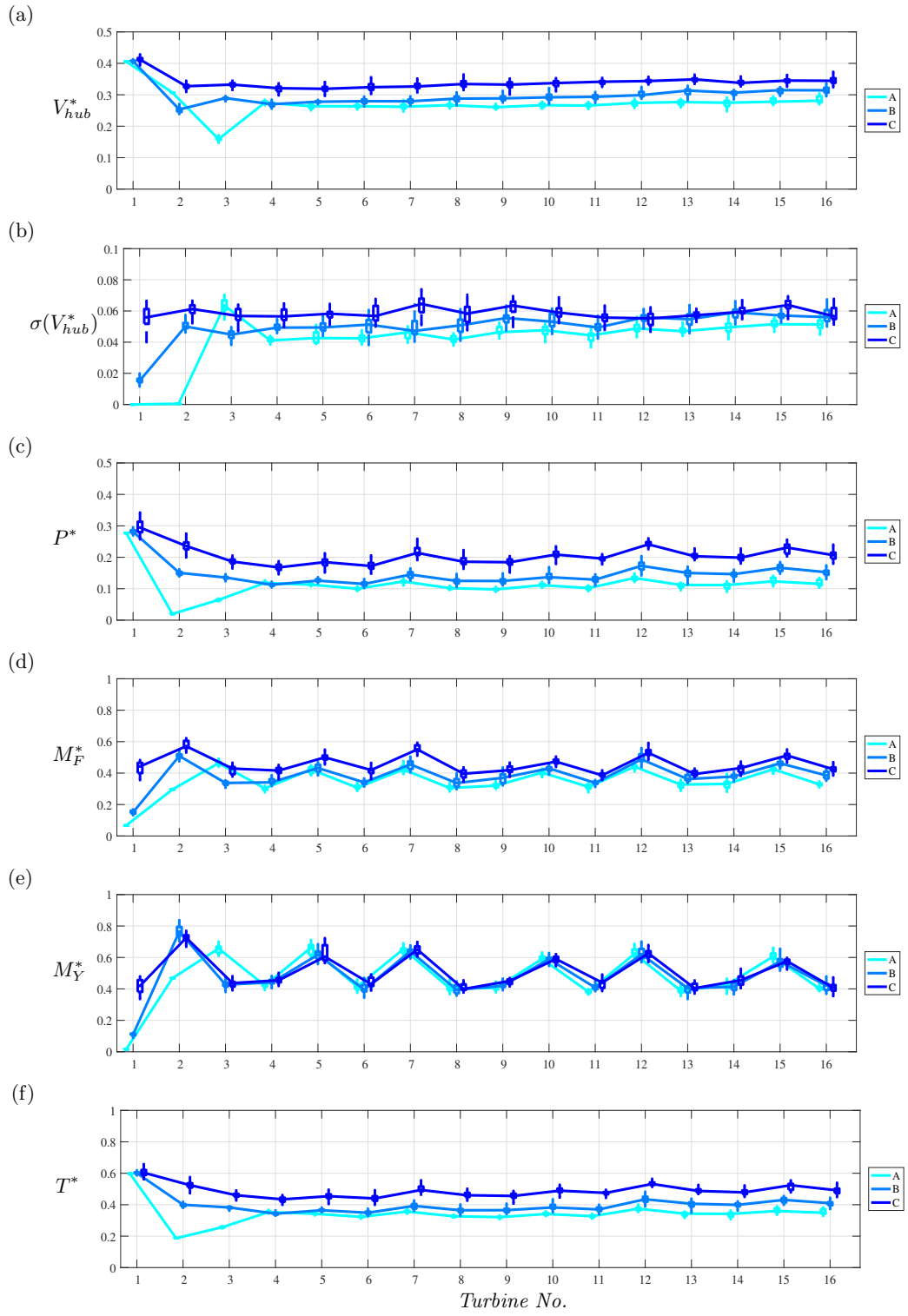

Figure 1. Boxplots of normalised 10min averages of (a) V^*_{hub}, standard deviation of (b) $\sigma(V^*_{hub})$, average of (c) P^* and 10min equivalent loads for (d) M^*_F, (e) M^*_Y, and (f) T^* for the 16 turbines in Simulations *A*-*C*. Lines connect the median of the distributions.

different 10min periods are included and reported for each simulation in the following, except

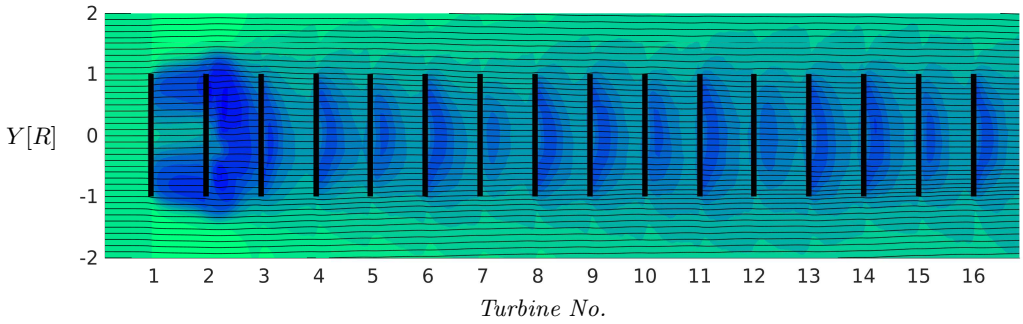

Figure 2. 10mins mean streamwise velocity and streamlines for simulation A.

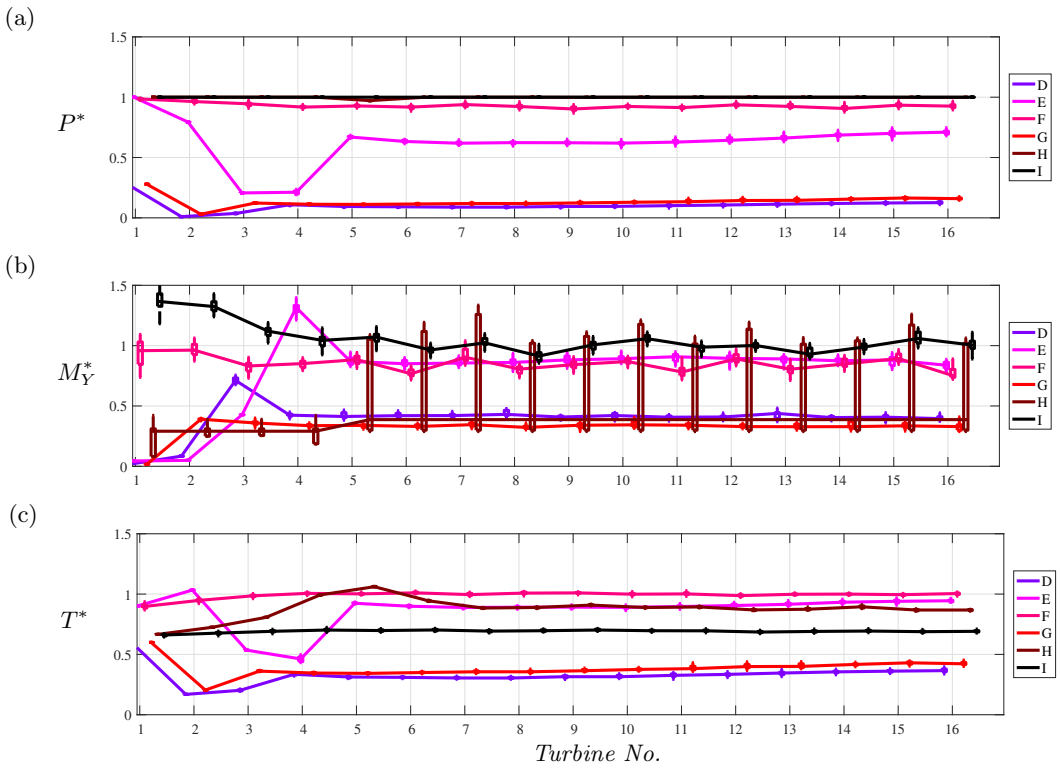

Figure 3. Boxplots of normalised 10min averages of (a) P^* and 10min equivalent loads for (b) M_Y^*, and (c) T^* for the 16 turbines in Simulations D-I. Lines connect the median of the distributions.

only 210 periods for Simulation H.

Figure 4 shows the aggregated statistics for each of the simulations (blue) in a polar plot, where each individual quantity is plotted at a given azimuthal position and the radial position shows the relative magnitude of the quantity compared to scaling parameters as described in Table 2. The standard deviations of the 510 periods are plotted as dashed lines. Simulation 0 without the effect of turbines is included in all plots for reference (black). The plots comprise a significant amount of information, but also give an immediate visual indication of the operating conditions for a given scenario, *i.e.*is the operation well balanced between power and loads or is it skewed either positively towards power or negatively towards loads. The reference is naturally skewed with higher velocities as well as higher ficticious power and thrust and very low loads.

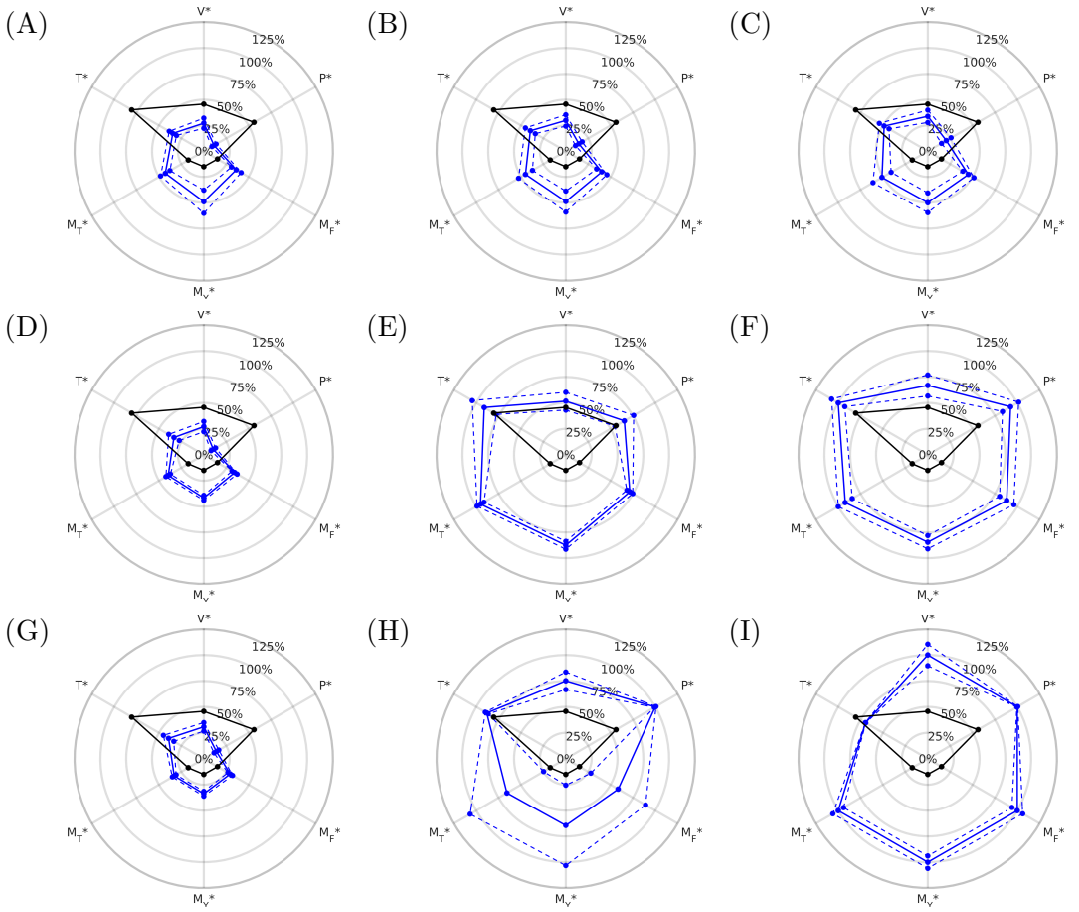

Figure 4. Polar plots showing mean velocity at hub height extracted $1R$ upstream, mean power production, mean 10min equivalent loads of flap, yaw, and tilt moments, and mean thrust. Statistics are based on the $7th$-$16th$ turbine. Quantities have been scaled by maximum values of all simulation for direct comparison. Broken lines show $\pm 1\sigma$. Simulation O with no turbines is shown for reference black.

Clearly, the majority of the scaling parameters comes from Simulation I, where the atmospheric turbulence intensity is large and the velocity is above rated, so the turbines are producing rated power. However, the highest thrust is experienced in Simulation F as the turbines operate around rated wind speed of 14m/s. The aforementioned increased spatial variability in Simulations A-C is evident in the larger standard deviations compared to Simulation D, which is very similar to Simulation A except a smaller lateral spacing. The largest variations in power occur for Simulation E and F with a freestream velocity just above rated, meaning that the waked turbines are constantly operating below rated. However, the largest variation in loads occur for Simulation H with high velocity and only self-generated turbulence. The variation could be related to large variations in the wake breakdown as described by Sørensen et al. [9].

Equivalent simulations, where only one parameter varies, are assembled in Figure 5. The effect of atmospheric turbulence in Simulations A-C shows (as expected) how increased atmospheric turbulence results in larger wake recovery, *i.e.* higher velocity and power, but also larger loads. However, the overall shape of the operation condition is maintained. Increased freestream velocity alters the operating condition significantly. The turbines below rated produce about

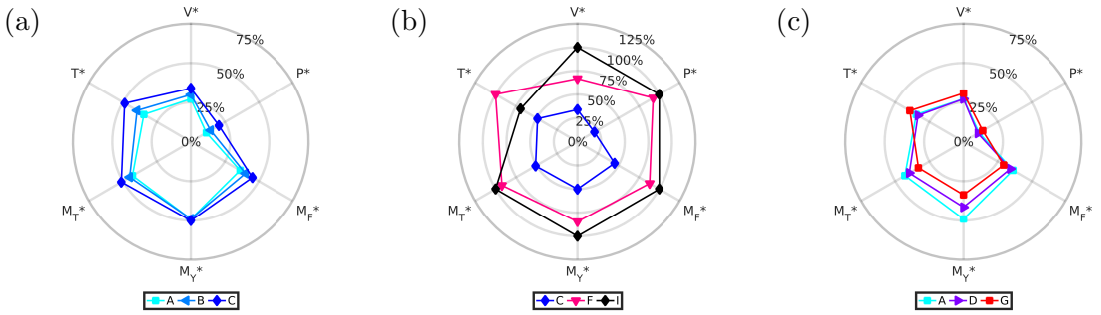

Figure 5. Comparing polar plots from Figure 4 showing effect of (a) atmospheric turbulence, (b) freestream velocity, and (c) spacing. Statistics are based on the $7th$-$16th$ turbine. Quantities have been scaled by maximum values of all simulation for direct comparison. Only mean normalised values are shown for clarity. Note, that the radial extent is changed in (a) and (c).

25% of rated power, but are exposed to approximately 50% of the maximum loading in the dataset. Turbines operating around rated experience the highest thrust and produced 92% of rated power with similar flapwise, yaw, and tilt loading around $85-92\%$ of maximum. For very high wind speed, the power and loads are at maximum, while thrust is reduced to 70%. Finally, the effect of spacing from Simulations A, D, and G show a slight increase in loads, particular yaw, when the lateral spacing is increased (A compared to D). However, increasing both streamwise and lateral spacing (D vs G) shows how the power production is increased, while loading is reduced.

3.4. Farm Layout

The full operational conditions can be used to elucidate on different farm layout scenarios similar to the work of *e.g.* Stevens et al. [27], who compared power production for different effective turbine spacings. Here, the equivalent loading and thrust on the turbines are added as a new dimension as the actual power is normalised by turbine spacing to yield a measure of the effective land use in $[W/m^2]$, see Figure 6. The five simulations with the same turbine arrangement are connected by a dashed line for reference as it covers a range of different operational conditions.

The data is concentrated in two regions, one below rated where power production is approximately $0.6-1.5W/m^2$ with corresponding loads of $30-50\%$ of the maximum equivalent load encountered in the total dataset for this specific turbine. The above rated region has a power production on the order of $6.6-8W/m^2$ and larger spread in the equivalent loads as the turbines operate around or above rated.

4. Conclusions

Ten simulations of large wind farms have been performed using a fully coupled LES and aeroelastic framework to form a database of full turbine operational conditions in terms of both production and loads. The performance is examined in terms of averaged power production and thrust, as well as 10min equivalent flapwise bending, yaw, and tilt moment loads. Certain scenarios operating below rated wind speed shows unexpected peaks in the loads, which occurs consistently across several simulations, but not immediately apparent or consistent in the flow statistics. The operating conditions of the farms are compared and the influence of atmospheric turbulence, freestream velocity, and turbine spacing is examined. The changes in equivalent loads and mean thrust are compared to the effective power production per area, which shows two distinct regions of waked turbine operation, corresponding to one below and one around/above

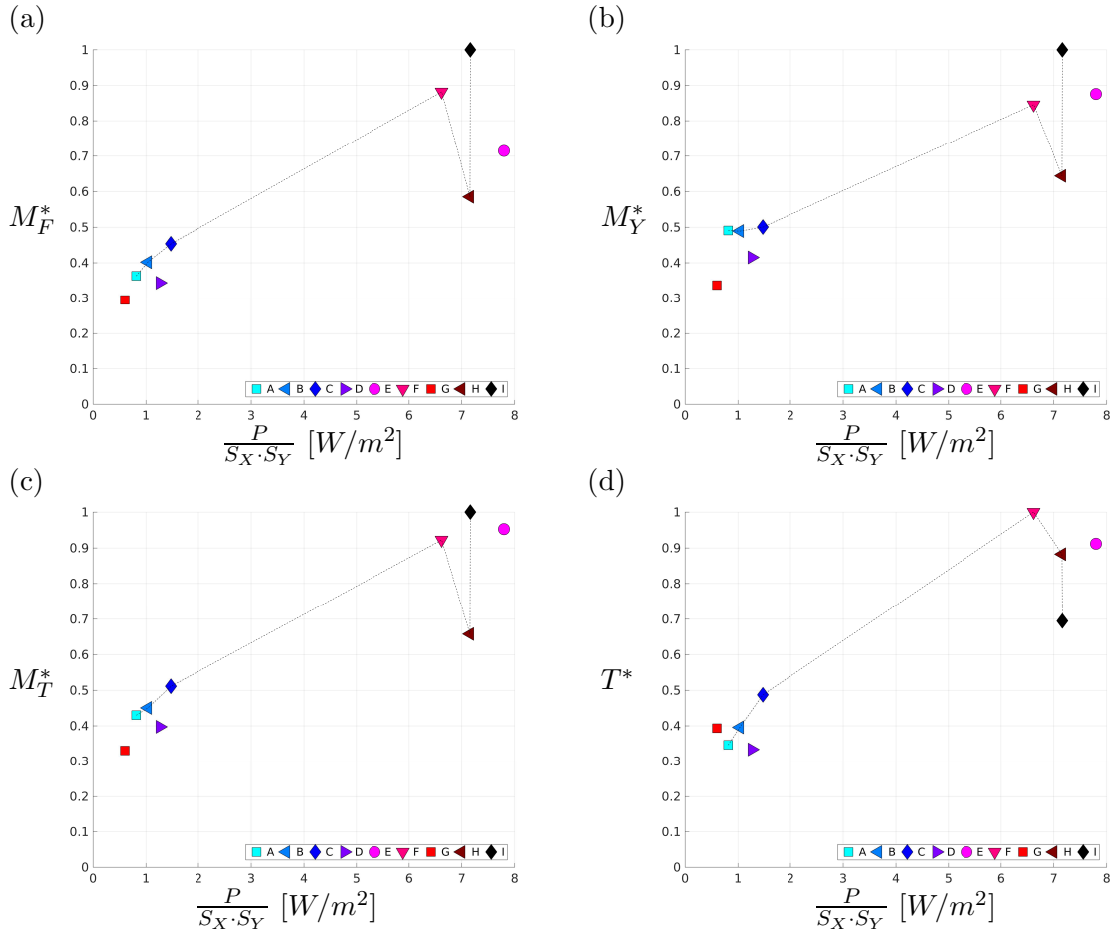

Figure 6. Equivalent (a) flapwise bending moment, (b) yaw moments, (c) tilt moment, and (d) mean thrust against actual power normalised by area. Simulations *A*-*C*, *F*, and *H*-*I* constituting the same wind farm is connected by a dashed line.

rated wind speeds. The database, albeit far from complete at present, provides detailed insights for designing large wind farms, *e.g.* the potential benefits of changing the farm layout to improve the levelized cost of energy by including loads. Furthermore, the database could be employed to alleviate particular unfavorable conditions by designing turbines and/or their controllers specifically to operate inside large wind farms under particular atmospheric conditions.

4.1. Acknowledgments

Acknowledgments

The analysed data has been gather during and as part of the following projects: Center for Computational Wind Turbine Aerodynamics and Atmospheric Turbulence (grant 2104-09-067216/DSF) (COMWIND: http://www.comwind.org), Nordic Consortium on Optimization and Control of Wind Farms funded by the Swedish Energy Agency, Eurotech Greentech Wind project, Winds2Loads, and CCA LES. Computer time was granted by the Swedish National Infrastructure for Computing (SNIC) and as well as on JESS (DTU). Furthermore, the proprietary data for Vestas' NM80 turbine has been used.

References

[1] Sørensen J N and Shen W Z 2002 *Journal of Fluids Engineering* **124** 393–399
[2] Calaf M, Meneveau C and Meyers J 2010 *Phys. Fluids* **22**
[3] Meyers J and Meneveau C 2012 *Wind Energy* **15** 305–317 ISSN 10991824, 10954244
[4] Meyers J and Meneveau C 2013 *J. Fluid Mech.* **715** 335–358
[5] Porté-Agel F, Wu Y T, Lu H and Conzemius R J 2011 *Journal of Wind Engineering and Industrial Aerodynamics* **99** 154–168
[6] Nilsson K, Ivanell S, Hansen M H, Mikkelsen R, Breton S P and Henningson D 2014 *Wind Energy*
[7] Troldborg N 2008 *Actuator Line Modeling of Wind Turbine Wakes* Ph.D. thesis DTU Mechanical Engineering, Technical University of Denmark, DTU, DK-2800 Kgs. Lyngby, Denmark Denmark
[8] Jha P K, Churchfield M J, Moriarty P J and Schmitz S 2014 *Journal of Solar Energy Engineering* **136** 031003–031003
[9] Sørensen J N, Mikkelsen R, Henningson D S, Ivanell S, Sarmast S and Andersen S J 2015 *Royal Society of London. Philosophical Transactions A. Mathematical, Physical and Engineering Sciences* **373** 20140071–20140071 ISSN 14712962, 1364503x
[10] Andersen S J 2013 *Simulation and Prediction of Wakes and Wake Interaction in Wind Farms* Ph.D. thesis Technical University of Denmark, Wind Energy.
[11] Storey R, Cater J and Norris S 2016 *Renewable Energy* **95** 31 – 42 ISSN 0960-1481 URL `http://www.sciencedirect.com/science/article/pii/S0960148116302518`
[12] Lee S, Churchfield M J, Moriarty P J, Jonkman J and Michalakes J 2013 *Journal of Solar Energy Engineering-transactions of the Asme* **135** 31001 ISSN 15288986, 01996231
[13] Larsen G C, Madsen H A, Bingöl F, Mann J, Ott S, Sørensen J N, Okulov V, Troldborg N, Nielsen M, Thomsen K, Larsen T J and Mikkelsen R 2007 Dynamic wake meandering modeling Tech. Rep. R-1607(EN) Risø-DTU Roskilde, Denmark
[14] Larsen G C, Madsen H A, Thomsen K and Larsen T J 2008 *Wind Energy* **11** 377–395
[15] Michelsen J A 1992 Basis3D – a Platform for Development of Multiblock PDE Solvers Tech. rep. Danmarks Tekniske Universitet
[16] Sørensen N N 1995 *General Purpose Flow Solver Applied to Flow over Hills* Ph.D. thesis Technical University of Denmark
[17] Øye S 11-12 April 1996 *Proceedings of 28th IEA Meeting of Experts Concerning State of the Art of Aeroelastic Codes for Wind Turbine Calculations. Available through International Energy Agency.* (Lyngby, Denmark: Danmarks Tekniske Universitet) pp 71–76
[18] Troldborg N, Sørensen J, Mikkelsen R and Sørensen N 2013 *Wind Energy* ISSN 1095-4244
[19] Mann J 1994 *Journal of Fluid Mechanics* **273** 141–168 ISSN 1469-7645
[20] Mann J 1998 *Probabilistic Engineering Mechanics* **13** 269–282 ISSN 0266-8920
[21] Ta Phuoc L, Lardat R, Coutanceau M and Pineau G 1994 Rechereche et analyse de modeles de turbulence de sous maille adaptes aux ecoulements instationnaires decolles.
[22] Aagaard Madsen H, Bak C, Schmidt Paulsen U, Gaunaa M, Fuglsang P, Romblad J, Olesen N, Enevoldsen P, Laursen J and Jensen L 2010 *The DAN-AERO MW Experiments* Denmark. Forskningscenter Risø. Risø-R (Danmarks Tekniske Universitet, Risø Nationallaboratoriet for Bæredygtig Energi) ISBN 978-87-550-3809-7
[23] Andersen S J, Sørensen J N, Mikkelsen R and Ivanell S 2016 *Journal of Physics: Conference Series. The Science of Making Torque from Wind 2016.* **753** ISSN 1742-6596
[24] Andersen S J, Sørensen J N and Mikkelsen R F 2017 *Philosophical Transactions of the Royal Society of London A: Mathematical, Physical and Engineering Sciences* **375** ISSN 1364-503X (*Preprint* `http://rsta.royalsocietypublishing.org/content/375/2091/20160107.full.pdf`) URL `http://rsta.royalsocietypublishing.org/content/375/2091/20160107`
[25] Andersen S J, Witha B, Breton S P, Sørensen J N, Mikkelsen R F and Ivanell S 2015 *Journal of Physics: Conference Series* **625** 012027 URL `http://stacks.iop.org/1742-6596/625/i=1/a=012027`
[26] Newman A J, Drew D A and Castillo L 2014 *Renewable Energy* **70** 129–141 ISSN 18790682, 09601481
[27] Stevens R J A M, Gayme D F and Meneveau C 2015 *Journal of Renewable and Sustainable Energy* **7**